aligned, highly multiplexable and high-contrast supertwisted displays have become feasible.

Figure 4 demonstrates the remarkably improved field of view of a photo-aligned four-domain TN displays (top) compared with the strongly angle-dependent brightness of a conventionally brushed, single-domain display (bottom). The angular dependence of the brightness of the two partially switched-on displays in Fig. 4 was measured in all four quadrants between vertical light incidence and 60° off-axis. The grey levels at vertical light incidence are identical for both displays, and correspond to 50% transmission in Fig. 3. Figure 4 shows that, instead of remaining constant, the brightness of the conventional display changes by nine grey levels (out of ten) within its first and third quadrant, whereas the brightness of the photoaligned four-domain display changes by only three grey levels within any of its four quadrants.

The remarkably improved viewing performance of photo-aligned multi-domain displays is further illustrated by the photographs in Fig. 5 which show the angular dependence of the grey level of a large single pixel at 70% vertical transmission of an LPP-aligned four-domain display (top) and of a PI-aligned single-domain display (bottom). The centre pictures were taken at vertical light incidence, the others at 40° in the four quadrants. The comparison is self explanatory. Also shown in Fig. 5 (ringed) is an enlarged view of a four-domain display pixel viewed at 40° in the first quadrant. This shows the four photopatterned and differently aligned TN-subpixels whose macroscopically averaged transmission accounts for the improved angular view of the photoaligned four-domain display.

We have shown that high-resolution (< 5 μm) liquid-crystal aligning patterns with defined and broadly adjustable bias tilt angles have become feasible with our linear photoalignment technology. For this reason, and because of its stability with respect to light and heat, photoalignment renders mechanical alignment with its detrimental generation of dust particles and electrostatic charges obsolete. LPP photoalignment of monomeric and polymeric liquid crystals not only improves the performance of existing displays, such as their viewing properties, but also opens up interesting new display configurations and non-display-related optically anisotropic devices[15], such as optically patternable interference filters, polarizers and optical retarders. □

Received 12 February; accepted 11 April 1996.

1. Schadt, M. & Helfrich, W. J. *Appl. Phys. Lett.* **18,** 127–128 (1971).
2. Cognard, J. *Molec. Cryst. liq. Cryst. Suppl. Ser.* **1,** 1–74 (1982).
3. Meyerhofer, D. *J. Appl. Phys.* **48,** 1179–1185 (1977).
4. Luo, F. C. in *Liquid Crystals* (ed Bahadur, B.) Vol. 1 (World Scientific, Singapore, 1990).
5. Yang, K. H. *Jap. J. appl. Phys. Lett.* **31,** 1603–1605 (1992).
6. Sumiyoshi, K., Takatori, K., Hirai, Y. & Kaneko, S. J. *Soc. for Information Display* **2/1** 31–33 (1994).
7. Kawata, Y., Takatoh, K., Hasegawa, M. & Sakamoto, M. *Liq. Cryst.* **16,** 1027–1036 (1994).
8. Hashimoto, T. *et al. Digest SID* '95 877–880 (Soc. for Information Display, Playa del Rey, CA, 1995).
9. Chen, J. *et al. Appl. Phys. Lett.* **67,** 1990–1992 (1995).
10. Schadt, M., Schmitt, K., Kozinkov, V. & Chigrinov, V. *Jap. J. appl. Phys.* **31,** 2155–2164 (1992).
11. Gibbons, W. M., Shannon, P. J., Sun, S. T. & Swetlin, B. J. *Nature* **351,** 49–50 (1991).
12. Schadt, M., Seiberle, H., Schuster, A. & Kelly, S. M. *Jap. J. appl. Phys.* **34,** 3240–3249 (1995).
13. Raynes, E. P. *Electron. Lett.* **10,** 141–142 (1974).
14. Scheffer, T. J. & Nehring, J. *Appl. Phys. Lett.* **45,** 1021–1023 (1984).
15. Schadt, M., Seiberle, H., Schuster, A. & Kelly, S. M. *Jap. J. appl. Phys. Lett.* **34,** 764–767 (1995).

Detection of nonlinear dynamics in short, noisy time series

Mauricio Barahona* & Chi-Sang Poon†‡

* Physics Department and † Harvard-MIT Division of Health Sciences and Technology, Massachusetts Institute of Technology, 77 Massachusetts Avenue, Cambridge, Massachusetts 02139, USA

THE accurate identification of deterministic dynamics in an experimentally obtained time series[1–5] can lead to new insights regarding underlying physical processes, or enable prediction, at least on short timescales. But deterministic chaos arising from a nonlinear dynamical system can easily be mistaken for random noise[6–8]. Available methods to distinguish deterministic chaos from noise can be quite effective, but their performance depends on the availability of long data sets, and is severely degraded by measurement noise. Moreover, such methods are often incapable of detecting chaos in the presence of strong periodicity, which tends to hide underlying fractal structures[9]. Here we present a computational procedure, based on a comparison of the prediction power of linear and nonlinear models of the Volterra–Wiener form[10], which is capable of robust and highly sensitive statistical detection of deterministic dynamics, including chaotic dynamics, in experimental time series. This method is superior to other techniques[1–6,11,12] when applied to short time series, either continuous or discrete, even when heavily contaminated with noise, or in the presence of strong periodicity.

Consider the usual description of a dynamical system as a 'black box' with input x_n and output y_n, at time $n = 1, \ldots, N$ in multiples of the sampling time τ. The discrete Volterra series is then a Taylor-like polynomial expansion of y_n in terms of $x_n, x_{n-1}, \ldots, x_{n-\kappa+1}$, where κ is the memory of the system. To overcome the computational intractability of the Volterra series, Wiener introduced an orthogonal formulation[13] assuming that x_n is a gaussian white noise sequence over an infinite time period. Korenberg's recasting of the expansion[14], on which our approach is based, relaxes these restrictions thereby allowing its application to finite and arbitrary signals.

For a dynamical system, either strictly autonomous or reformulated as such, we propose a closed-loop version of the Volterra series in which the output y_n feeds back as delayed input (that is, $x_n \equiv y_{n-1}$). Within this framework, we analyse univariate time series by using a discrete Volterra–Wiener–Korenberg series of degree d and memory κ as a model to calculate the predicted time series y_n^{calc}:

$$y_n^{\text{calc}} = a_0 + a_1 y_{n-1} + a_2 y_{n-2} + \cdots + a_\kappa y_{n-\kappa} + a_{\kappa+1} y_{n-1}^2 + a_{\kappa+2} y_{n-1} y_{n-2} + \cdots + a_{M-1} y_{n-\kappa}^d = \sum_{m=0}^{M-1} a_m z_m(n) \quad (1)$$

where the functional basis $\{z_m(n)\}$ is composed of all the distinct combinations of the embedding space coordinates[15] $(y_{n-1}, y_{n-2}, \ldots, y_{n-\kappa})$ up to degree d, with a total dimension $M = (\kappa + d)!/(d!\kappa!)$. Thus, each model is parametrized by κ and d, which correspond to the embedding dimension and the degree of nonlinearity of the model, respectively. The coefficients a_m are recursively estimated through a Gram–Schmidt procedure[14] from linear and nonlinear autocorrelations of the data series itself. The calculations can be readily performed on a workstation.

The short-term prediction power of a model is then measured by the standard one-step-ahead prediction error

$$\varepsilon(\kappa, d)^2 \equiv \frac{\sum_{n=1}^{N} (y_n^{\text{calc}}(\kappa, d) - y_n)^2}{\sum_{n=1}^{N} (y_n - \bar{y})^2} \quad (2)$$

where $\bar{y} = 1/N \sum_{n=1}^{N} y_n$ and $\varepsilon(\kappa, d)^2$ is in effect a normalized variance of the error residuals. We now search for the best

‡To whom correspondence should be addressed.

model $\{\kappa_{opt}, d_{opt}\}$ that minimizes the following information criterion[16] in accordance with the parsimony principle:

$$C(r) = \log \varepsilon(r) + r/N \quad (3)$$

where $r \in [1, M]$ is the number of polynomial terms of the truncated Volterra expansions from a certain pair $\{\kappa, d\}$.

The numerical procedure is as follows: for each data series, obtain the best linear model by searching for κ^{lin} which minimizes $C(r)$ with $d = 1$. Repeat with increasing κ and $d > 1$, to obtain the best nonlinear model. Likewise, obtain the best linear and nonlinear models for surrogate randomized data sets with the same autocorrelation (and power spectrum) as the original series[3,5]. This results in four competing models with error standard deviations ε^{lin}_{orig}, ε^{nl}_{orig}, ε^{lin}_{surr} and ε^{nl}_{surr}.

From above, the presence of nonlinear determinism is indicated if $d_{opt} > 1$. Further corroboration is obtained with the following objective statistical criteria: for models with gaussian residuals, a standard F-test will serve to reject, with a certain level of confidence, the hypothesis that nonlinear models are no better than linear models as one-step-ahead predictors. This gaussian assumption was verified throughout our analysis by using a χ^2-test with a 99% cutoff. Alternatively, the results are confirmed by using the nonparametric Mann–Whitney rank-sum statistic, which does not depend on the gaussian assumption[3]. Under this scheme, the relevance of nonlinear predictors is established when the best nonlinear model from the original data is significantly more predictive than both (1) the best linear model from the data series, and (2) the best linear and nonlinear models obtained from the surrogate series, that is, ε^{lin}_{orig}, ε^{nl}_{surr}, $\varepsilon^{lin}_{surr} > \varepsilon^{nl}_{orig}$ in the statistical sense.

Two points are noteworthy. First, because surrogate data are generated by preserving only the linear autocorrelation function of the data series (nonlinear autocorrelations are randomized), the addition of nonlinear terms does not increase the prediction power. As expected, $\varepsilon^{nl}_{surr} \approx \varepsilon^{lin}_{surr}$ and surrogate data are always best approximated by a linear model.

Second, when dealing with continuous signals, the time delay τ for the embedding (or optimal sampling rate) is another free parameter to be determined[17]. For detection purposes, the optimal time delay τ_{opt} may be chosen so as to maximize the difference between ε^{lin}_{orig} and ε^{nl}_{orig}. The value of τ_{opt} is bounded by two limits. On one hand, if $\tau \gg \tau_{opt}$ (undersampling) all four models (linear and nonlinear, original or surrogate) will have similarly small prediction powers and nonlinearity cannot be detected. On the other hand, for an oversampled data series with a small step size ($\tau \ll \tau_{opt}$), the linear correlation of the embedding is so large that linear models always prevail. Within the range of acceptable time delays where τ_{opt} lies, generally $\varepsilon^{lin}_{orig} \approx \varepsilon^{lin}_{surr}$; that is, when optimally sampled, the prediction power of the linear model of a continuous signal derives mainly from its autocorrelation function. This equivalence of linear models from original and surrogate data holds for discrete maps as well. Consequently, and in contrast with other methods, surrogate data play only a confirmatory role in our procedure.

We have tested our algorithm with a wide variety of short time series, typically 1,000 points long. As a preliminary trial, we verified the method with several linear signals which, in some cases, proved to be non-recognizable by some of the existing methods (see discussions in refs 3 and 8). The examples included: white gaussian and coloured $1/f^{\alpha}$ noises[7]; an autoregressive linear random process[3]; periodic sinusoidal and nonsinusoidal series (see Theiler in ref. 8); as well as a quasiperiodic signal from a torus with two frequencies (Paluš in ref. 8). In all cases the method yielded $\varepsilon_{lin} \leqslant \varepsilon_{nl}$ and the linear hypothesis could not be rejected. The same conclusion was reached in the presence of noise or when an *a posteriori* nonlinear transformation was performed on the original linear data[5].

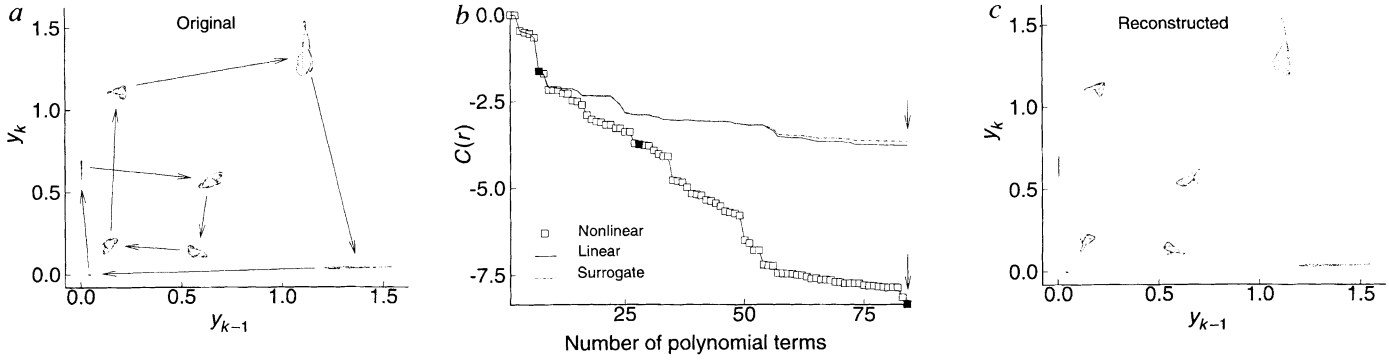

FIG. 1 *a*, Embedding reconstruction of an ecological model[9]: $x_k = \lambda y_{k-1}\exp(-0.001(y_{k-1} + x_{k-1}))$; $y_k = 0.2x_{k-1}\exp(-0.07(y_{k-1} + x_{k-1})) + 0.8y_{k-1}\exp(-0.05(y_{k-1} + 0.5x_{k-1}))$ with $\lambda = 118$. The trajectory evolves in an attractor comprised of fractals in several disconnected domains and visits each of them in a periodic manner as indicated by the arrows. This strong periodicity makes detection of the chaotic component difficult. *b*, $C(r)$ (see equation (3); r is the number of polynomial terms) for a set of nonlinear, linear and surrogate data models for a time series (1,000 points) from the same ecological model, no noise added. Linear and surrogate models with $d = 1$ and differing κ (see text) are represented. The nonlinear models are complete (■) or truncated (□) Volterra series with fixed $\kappa = 6$ and varying d. Optimal nonlinear, linear and surrogate models are indicated by the arrows. Here $F_{calc} = (\varepsilon^{lin}_{orig})^2/(\varepsilon^{nl}_{orig})^2 = 9,387 \gg F(0.01, 915, 915) = 1.17$ Alternatively, the Mann–Whitney statistic is $Z = -37.13 \ll -2.33$, the value of the inverse normal cumulative density function for $\alpha = 0.01$. Similarly, the information criterion $C(r)$ indicates that $d_{opt} > 1$. From these three criteria we deduce the nonlinear component is significant. *c*, Attractor propagated from a model ($\kappa = 2$, $d = 8$) obtained with the algorithm. It captures the general shape and subfractal structure of the attractor of the original non-Volterra model. *d*, Plot of $1/F_{calc}$ versus the percentage of added coloured noise for the same ecological example. The noise percentage is defined as the ratio of the standard deviations of the additive random series and the original data. The discontinuous line indicates the 99% confidence interval. The nonlinear deterministic component can be reliably detected even in the presence of ~ 50% correlated noise. Similar results (not shown) are obtained for the connected fractal with $\lambda = 140$.

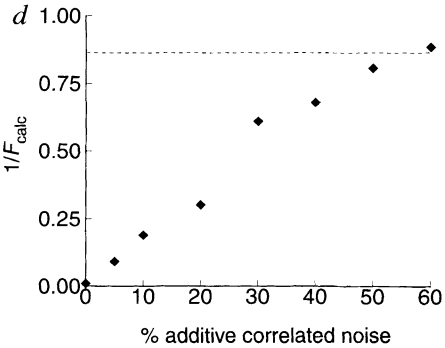

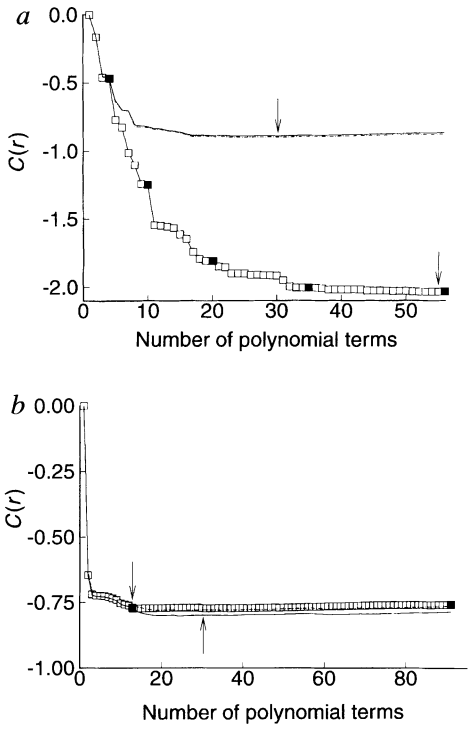

FIG. 2 *a*, As Fig. 1*b*, but for an experimental time series (1,000 points) of emission of an NH_3 laser from an apparatus designed to produce Lorenz-like chaos (series A from ref. 8). In this case $F_{calc} = 10.23 > F(0.01, 968, 944) = 1.16$, and the nonparametric Mann–Whitney statistic is $Z = -24.60 < -2.33$. Both criteria (and $C(r)$) indicated that the nonlinear component is significant. *b*, As *a*, but for an experimental time series (1,874 points) of the intensity of a variable dwarf star (segments 1 and 2 of series E from ref. 8) in which linear superposition of modes had been presumed and was to be verified. Not only is $d_{opt} = 1$ but the hypothesis of nonlinearity may be rejected with a 94% confidence level as $1/F_{calc} = 1.08 \approx F(0.06, 1855, 1783)$.

Table 1 summarizes some of the results for numerically generated nonlinear examples. It is important to emphasize the diversity of the data sets. For example, most of the discrete series (except the Hénon and logistic maps) have non-polynomial, non-Volterra functional forms. The detection algorithm worked equally well with continuous systems, including those that evolve around several ghost centres (Lorenz, Duffing); high-dimensional systems (as in series D (ref. 8), with a dimension of 9); and chaotic series from nonlinear delayed feedback mechanisms (Mackey–Glass equation) with implicit dimension of seven.

We also examined the robustness of our method in the presence of noise by adding to all the nonlinear examples white and/or coloured measurement noises—the latter with the same autocorrelation as the original series (Table 1). Even with such short series, nonlinearity was detected under high levels of noise ($\sim$ 40–75%) comparable to those achieved by other methods with much longer ($\sim$16,000 points) series[3].

TABLE 1 Results of algorithm tests

Discrete systems	%	Continuous systems	%
Logistic map	70	Rössler	75
Hénon map	70	Duffing	40
Ikeda map	65	Lorenz II (ref. 3)	50
Ecological model[9]	50	Series D (ref. 8)	50
Non-chaotic fractal[21]	25	Mackey–Glass[5]	15

List of numerically generated nonlinear examples and approximate maximum percentages of correlated noise that can be added to a 1,000-points-long series before the nonlinear component is no longer detected with a 99% cutoff. These maximum values increase for longer data series.

As an example of the power of the algorithm, Fig. 1 shows results for an ecological model whose chaotic component, obscured by strong periodicity, has eluded detection by some of the existing methods even in the absence of noise[9]. In contrast, our technique—without any reprocessing of the data—detected the presence of nonlinearity even when the series was corrupted by $\sim 50\%$ additive correlated noise. Moreover, the algorithm is robust against contamination of the signal with random spikes (Poisson impulses) of intensities comparable to the signal amplitude and density up to 0.02.

Dynamic noise—random noise recycled by the dynamics of the system—is a major source of variability in feedback systems[18]. We addressed this issue by numerically introducing white and/or coloured dynamic noise in Hénon and Ikeda maps with boundary constraints to keep the trajectories in the attractors. Encouragingly, the method detected nonlinearity up to similar levels of noise as for the purely additive case, that is, $\sim 80\%$ and $\sim 70\%$ respectively.

Finally, we tested our algorithm with two benchmark experimental series (Fig. 2); the results are in agreement with published conclusions[8].

Some questions remain concerning the significance of the models so obtained. Although the choice of model selection criterion is not critical for the present purposes, the reliability of the resulting models as long-term predictors (for example, Fig. 1*c*) is highly dependent on the chosen criterion, the nature of the time series and the amount of noise present (M.B. and C.-S.P., unpublished work). The procedure can be extended to non-polynomial functional bases[19] or multivariate series. But these approaches may not be feasible for large-scale functional expansions unless efficient algorithms (such as the recursive one proposed here become available. New directions for the method, including iterative refinement of models with shadowing[20] or other noise-reduction techniques, may prove useful for modelling in the presence of noise and full detection of chaos. The demonstrated robustness of the technique in a wide variety of test examples suggests its possible applicability to general experimental data. □

Received 13 November; accepted 3 April 1996.

1. Sugihara, G. & May, R. M. *Nature* **344,** 734–741 (1990).
2. Casdagli, M. *Physica* D**35,** 335–356 (1989).
3. Kennel, M. B. & Isabelle, S. *Phys. Rev.* A**46,** 3111–3118 (1992).
4. Theiler, J., Eubank, S., Longtin, A., Galdrikian, B. & Farmer, J. D. *Physica* D**58,** 77–94 (1992).
5. Kaplan, D. T. & Glass, L. *Physica* D**64,** 431–454 (1993).
6. Grassberger, P. & Procaccia, I. *Physica* D**9,** 189–208 (1983).
7. Osborne, A. R. & Provenzale, A. *Physica* D**35,** 357–381 (1989).
8. Weigend, A. S. & Gershenfeld, N. A. (eds) *Time Series Prediction* (Santa Fe Inst. Studies in the Sciences of Complexity, Vol. XV, Addison-Wesley, Reading, MA, 1994).
9. Cazelles, B. & Ferriere, R. H. *Nature* **355,** 25–26 (1992).
10. Marmarelis, V. Z. (ed.) *Advanced Methods of Physiological System Modeling* Vol. II (Plenum, New York, 1988).
11. Grassberger, P. & Procaccia, I. *Phys. Rev.* A**28,** 2591–2593 (1983).
12. Sano, M. & Sawada, Y. *Phys. Rev. Lett.* **55,** 1082–1085 (1985).
13. Wiener, N. *Nonlinear Problems in Random Theory* (Wiley, New York, 1958).
14. Korenberg, M. J. *Ann. biomed. Eng.* **16,** 123–142 (1988).
15. Takens, F. in *Dynamical Systems and Turbulence* (eds Rand, D. A. & Young, L. S.) 336–381 (Lecture Notes in Mathematics Vol. 898, Springer, Berlin, 1981).
16. Akaike, H. *IEEE Trans. Auto. Control* **19,** 716–723 (1974).
17. Fraser, A. M. & Swinney, H. L. *Phys. Rev.* A**33,** 1134–1140 (1986).
18. Glass, L. & Malta, C. P. *J. theor. Biol.* **145,** 217–223 (1990).
19. Crutchfield, J. P. & MacNamara, B. S. *Complex Systems* **1,** 417–452 (1987).
20. Hammel, S. M. *Phys. Lett.* A**148,** 421–428 (1990).
21. Grebogi, C., Ott, E., Pelikan, S. & Yorke, J. A. *Physica* D**13,** 261–268 (1984).

ACKNOWLEDGEMENTS. We thank L. Glass and A. L. Goldberger for helpful comments. M.B. was supported by a Spanish MEC-Fulbright Fellowship. C-S.P. was supported in part by grants from the NSF, ONR and NHLBI.